

# Lawrence Berkeley National Laboratory

## LBL Publications

### Title

Polymer-Derived and Sodium Hydroxide-Treated Silicon Carbonitride Material as Anodes for High Electrochemical Performance Li-ion Batteries

### Permalink

<https://escholarship.org/uc/item/7qg9z552>

### Journal

ChemistrySelect, 1(2)

### ISSN

2365-6549

### Authors

Feng, Yan  
Wei, Yuzhen  
Jia, Zhe  
[et al.](#)

### Publication Date

2016-02-01

### DOI

10.1002/slct.201600046

Peer reviewed

# **Polymer-derived and NaOH-treated Silicon Carbonitride Material as Anodes for High Electrochemical Performance Li-ion Batteries**

Yan Feng<sup>1, 2, \*</sup>, Yuzhen Wei<sup>1</sup>, Zhe Jia<sup>2</sup>, Yuliang Zhang<sup>1</sup>, Vincent Battaglia<sup>2</sup> and Gao Liu<sup>2, \*</sup>

<sup>1</sup> Key Laboratory of Inorganic-Organic Hybrid Functional Material Chemistry, Ministry of Education; Tianjin Key Laboratory of Structure and Performance for Functional Molecules; College of Chemistry, Tianjin Normal University, Tianjin 300387, China; E-mail: hxyfy@mail.tjnu.edu.cn (Y.F.); 1048866580@qq.com (Y.W.); 563173667@qq.com (Y. Z.)

<sup>2</sup> Energy Storage and Distributed Resources, Lawrence Berkeley National Laboratory, Berkeley, California 94720, United States; zjia@lbl.gov (Z. J.); vsbattaglia@lbl.gov (V. B.); gliu@lbl.gov (G. L.)

\* Authors to whom correspondence should be addressed; E-mails: hxyfy@mail.tjnu.edu.cn (Y.F.); gliu@lbl.gov (G.L.); Tel.: +86-22-23766515 (Y.F.); +1-510-4867207 (G. L.); Fax: +1-510-4867303 (G. L.)

**Abstract:** Polymer-derived and micro-cracked silicon carbonitride (SiCN) materials have been successfully synthesized via pyrolyzing from poly(diphenylcarbodiimide) and post-treating with different molar concentration of NaOH aqueous solution (0.2-5.0 mol L<sup>-1</sup>). The as-prepared SiCN materials have been used as anodes for lithium ion batteries. Electrochemical charge-discharge measurements indicate that the SiCN with the 0.5 mol L<sup>-1</sup> of NaOH treating (SiCN-0.5-NaOH) shows the best electrochemical performance. It exhibits a high initial specific deintercalation capacity of 1159.5 mAh g<sup>-1</sup> and stable capacity of 900 mAh g<sup>-1</sup> at 0.1 C current density (40 mA g<sup>-1</sup>), which is 8.1 times as large as untreated SiCN anode, and 3.1 times as large as the traditional graphite anode. In addition, SiCN-0.5-NaOH anode exhibits excellent high-rate performance. At 2C current density (800 mA g<sup>-1</sup>), the extracted capacity stables above 600 mAh g<sup>-1</sup>, showing much greater performance than the traditional graphite anode. Transmission electron microscope (TEM), Fourier transform infrared spectra (FTIR) and X-ray photoelectron spectrometer (XPS) results show that nonconductive Si<sub>3</sub>N<sub>4</sub> was removed from SiCN matrix by the chemical reaction with NaOH solution. The morphology and structure measurements show its surface is rough, and many micro-sized cracks are formed. The special performances of NaOH-treated SiCN anodes are attributed to following two possible reasons: the one is non-conductive Si<sub>3</sub>N<sub>4</sub> phase elimination from SiCN matrix by NaOH treatment; the other is the lithium ion transfer channel enrichment and volume expansion buffered by the formation of micro-cracks. Our treating method for high conductive SiCN materials can be generalized to other silicon-based material anodes for the application of Li-ion batteries.

**Keywords:** polymer-derived; silicon carbonitride; sodium hydroxide treatment; anode; Li-ion batteries

## 1. Introduction

Lithium ion batteries, as one of the promising candidate for new energy storage devices, have received great attention in recent years because of the increasing energy consumption and environment concerns resulted from fossil fuel burning in our world [1-3]. There is an urgent need for new electrode materials to face up growing safety, capacity and high rate performances requirement in battery industry [4, 5]. Even though gained great success during the past decade, the current graphite anode is characterized by low capacity (372 mAh g<sup>-1</sup> in theory and 340 mAh g<sup>-1</sup> in practical use) and low kinetics at high charge-discharge rate, limiting its use in high energy and power density applications [6].

As one of alternative anode materials, polymer-derived silicon carbonitrides (SiCN) have been studied in the middle of 1990s [7, 8], and a rebirth of research boom is being spurred since 2006 [9-25]. They are prepared by the controlled pyrolysis of inorganic-organic hybrid polymers containing Si, H, C and N in an inert atmosphere at relatively low temperatures [26]. They are featured as amorphous materials with carbon content dependent electrical conductivity, excellent thermal persistence, high strength, and oxidative and corrosive resistance [27-30]. They are promising for safe use under extreme conditions. Lithium ion batteries with SiCN anode show enhanced reversible capacity (400-500 mAh g<sup>-1</sup>) and relatively electrochemical cycling stability as compared to conventional graphite-based anode [31]. As one of the novel silicon-based anodes, it has unique Si-C-N network structure, in which embed numerous lithiation sites from the dangling bonds of silicon, and the space between nano-sized graphene layers. All of them are beneficial to the insertion/exaction of the lithium ions [24].

Despite the high first extracted capacity of SiCN in the range of 700-1000 mAh g<sup>-1</sup>, the irreversible capacity at first cycle is large and the coulombic efficiency is low (about 40-50%), which maybe caused by its low electrical conductivity and the volume expansion during charge-discharge process [9, 10]. To resolve this issue, decreasing the non-conductive component and increasing carbon content in SiCN matrix are two feasible strategies. For the former, removing the non-conductive Si<sub>3</sub>N<sub>4</sub> phase — one of the three amorphous phases (Si<sub>3</sub>N<sub>4</sub>, SiC and graphite) in well-prepared SiCN matrix — is the efficient way to improve the integral conductivity of SiCN [30, 31]. For the latter, using carbon-rich polymer as the precursor will improve the carbon content in the final product of SiCN effectively [32-33].

Hence, in this paper, we focus on the preparation of micro-cracked SiCN materials without Si<sub>3</sub>N<sub>4</sub> phase by carbon-rich polymer precursor via chemical synthesis. In our previous research, we found that hydrofluoric acid can react with Si<sub>3</sub>N<sub>4</sub> phase by etching SiCN matrix, leading to enhanced capacity and cycle stability [25]. However, the hydrofluoric acid is toxic and harmful to the environment. To solve this problem, we employ sodium hydroxide solution instead of hydrofluoric acid, and design a nontoxic and facile chemical method to remove the Si<sub>3</sub>N<sub>4</sub> phase from the SiCN matrix. In addition, an extra benefit comes as an additional effect of micro voids and cracks is expected to form on the surface and bulk of SiCN material which will not only provide improved ion transport channels for the Li<sup>+</sup> intercalation/deintercalation, but also buffer the volume expansion during cycling. The SiCN materials without nonconductive phase Si<sub>3</sub>N<sub>4</sub> are expected to exhibit excellent electrochemical performances as anodes for lithium ion batteries.

## 2. Results and discussion

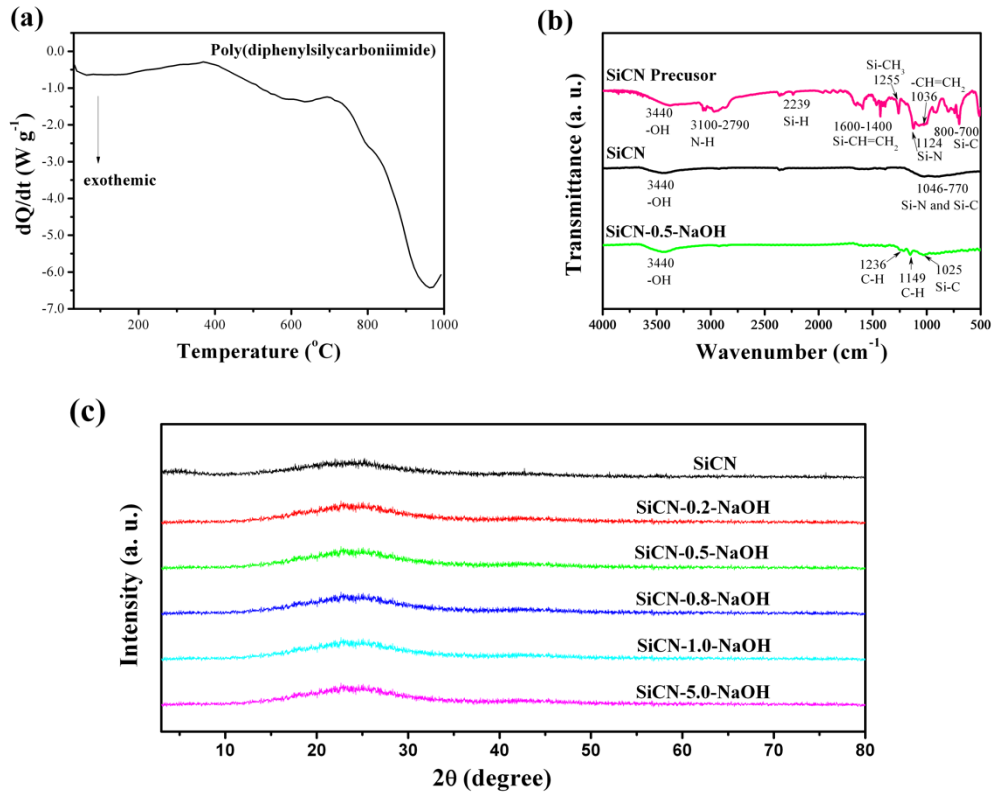


**Figure 1.** (a) DSC of the cross-linked SiCN polymer precursor; (b) FTIR spectra of the SiCN polymer precursor, SiCN, and NaOH-treated SiCN (SiCN-0.5-NaOH); (c) XRD patterns of the SiCN, and NaOH-treated SiCN materials (SiCN-x-NaOH, x=0.2, 0.5, 0.8, 1.0, 5.0).

The thermal behavior of polymer precursor was analyzed by differential scanning calorimetry (DSC) as shown in Figure 1a. As indicated by the DSC curve, we can see the cross-linked SiCN polymer precursor, poly(diphenylcarbodiimide), started to decompose at 400 °C. From the DSC curve, the polymer has one exothermic peak at 400-700 °C, which corresponds to the decomposition of organic groups and carbon framework from the polymer precursor. After heating at 1000 °C, all SiCN polymer precursors are transformed into inorganic SiCN material.

To further investigate the polymer precursor to ceramic transformation and the NaOH

effect on the changes of internal bonds of SiCN, FTIR are employed as shown in Figure 1b. Before pyrolysis, the SiCN precursor has many organic groups of -OH, N-H, Si-H, Si-CH=CH<sub>2</sub>, Si-CH<sub>3</sub>, -CH=CH<sub>2</sub>, Si-N, and Si-C. After pyrolysis, only Si-N and Si-C bonds appear in the SiCN matrix, the weak absorption for -OH bond is attributed to a small amount of absorbed water. Obviously, during the pyrolytic process, the polymer precursor was transferred into a ceramic, which involves breaking of above organic bonds, resulting in the absence or decrease of intensity with corresponding peaks in the FTIR spectrum of SiCN. After NaOH-treating, the Si-N bond is absent in Figure 1b, confirming the reaction completion.

In the XRD pattern of untreated SiCN material (Figure 1c), the diffraction peaks are broad, which suggests an amorphous structure. The Si<sub>3</sub>N<sub>4</sub> and SiC crystal lattices that are observed in the TEM images (Figure 3) are not found in the XRD pattern. This is because the Si<sub>3</sub>N<sub>4</sub> and SiC phase are covered up by the large amount of amorphous phases because their low crystallinity. It is interesting to compare the XRD pattern before and after NaOH treatment. There is no noticeable change from the pristine SiCN to the NaOH-treated SiCN materials, which indicates that the amorphous structure remained original state and no new phase was formed in the SiCN matrix during the NaOH-treating process.

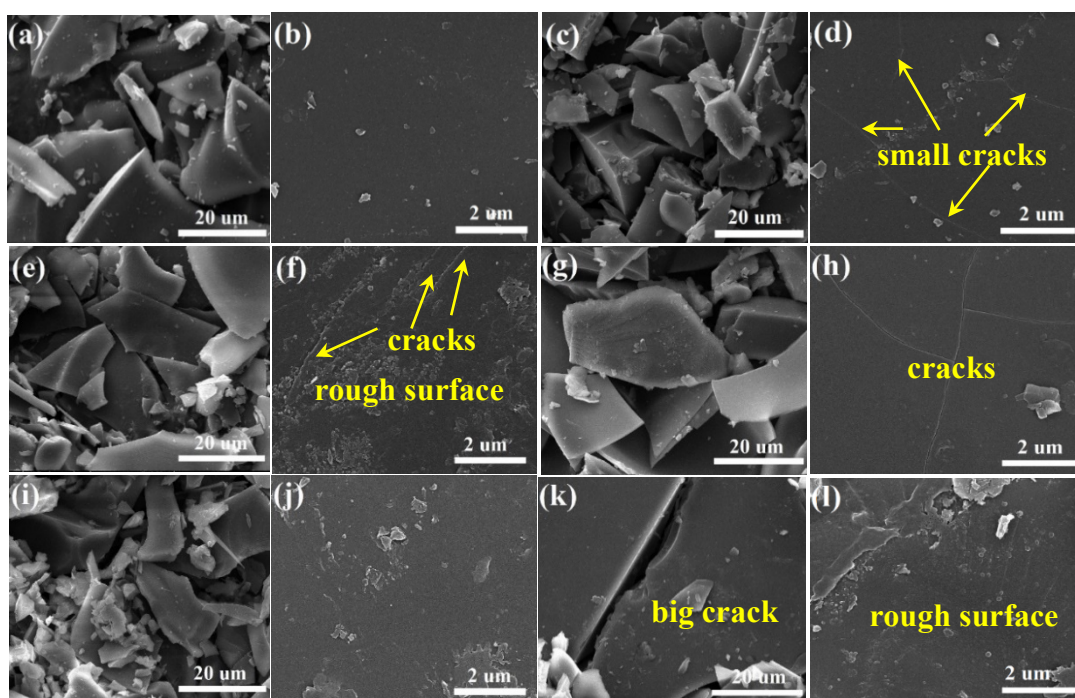


**Figure 2.** SEM images of SiCN (a, b), and SiCN-0.2-NaOH (c, d), SiCN-0.5-NaOH (e, f), SiCN-0.8-NaOH (g, h), SiCN-1.0-NaOH (i, j), SiCN-5.0-NaOH (k, l).

The morphologies of the untreated SiCN and NaOH-treated SiCN materials were characterized by SEM with the images shown in Figure 2. As shown in Figure 2a, c, e, g, k, and i, the particle sizes of all the heterogeneous SiCN materials are within the range from 5 to 20  $\mu\text{m}$ . The surfaces of the untreated SiCN are dense and rigid (Figure 2a and b), while the surfaces of the NaOH-treated SiCN are rough and loose with a lot of micro-cracks (Figure 2d, f, h, j and l). Consequently, the unique surface morphology was formed during the NaOH-treating process. With the increasing of the NaOH concentration, the surface become rougher and the cracks become bigger. As shown in the SEM images, the cracks in SiCN with 0.2 mol L<sup>-1</sup> NaOH-treating (Figure 2d) are slender and short, while they are wider and longer in SiCN with 0.8 mol L<sup>-1</sup> NaOH-treating (Figure 2k). When the concentration of NaOH increases to 5 mol L<sup>-1</sup>, the even longer and wider crack can be clearly observed (Figure 2k). These micro-cracks and voids lead to large surface areas of

the SiCN materials that were further proved by N<sub>2</sub> adsorption-desorption analysis. The SiCN-0.5-NaOH has a BET surface area of 5.5722 m<sup>2</sup>/g, which is 12.37 times as large as that of the SiCN without NaOH treatment.

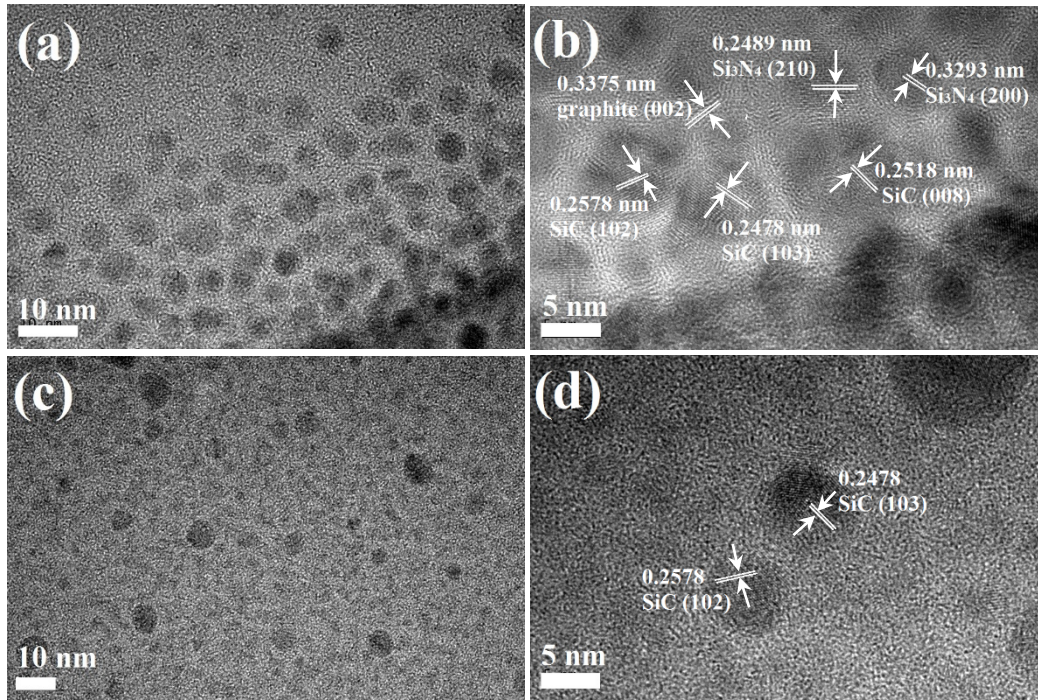


**Figure 3.** TEM images of SiCN (a, b) and SiCN-0.5-NaOH materials (c, d).

TEM images of the SiCN and SiCN-0.5-NaOH materials are shown in Figure 3. It can be clearly seen that the nano-sized crystals are dispersed evenly in the SiCN matrix (Figure 3a and c). In the structure of untreated SiCN (Figure 4b), apparently, the crystal lattices of SiC, Si<sub>3</sub>N<sub>4</sub> and graphite are dispersed unevenly. It is worth to note that no graphite and Si<sub>3</sub>N<sub>4</sub> lattice is observed in the TEM image of NaOH-treated SiCN material. Both graphite and Si<sub>3</sub>N<sub>4</sub> must be either transformed or eliminated by chemical reaction. For graphite, it is possible that it transforms to amorphous carbon. However, for Si<sub>3</sub>N<sub>4</sub>, the only possibility is that it is eliminated by the reaction with NaOH during the treatment (Si<sub>3</sub>N<sub>4</sub> and NaOH maybe react as the equation (1) shown in the following).



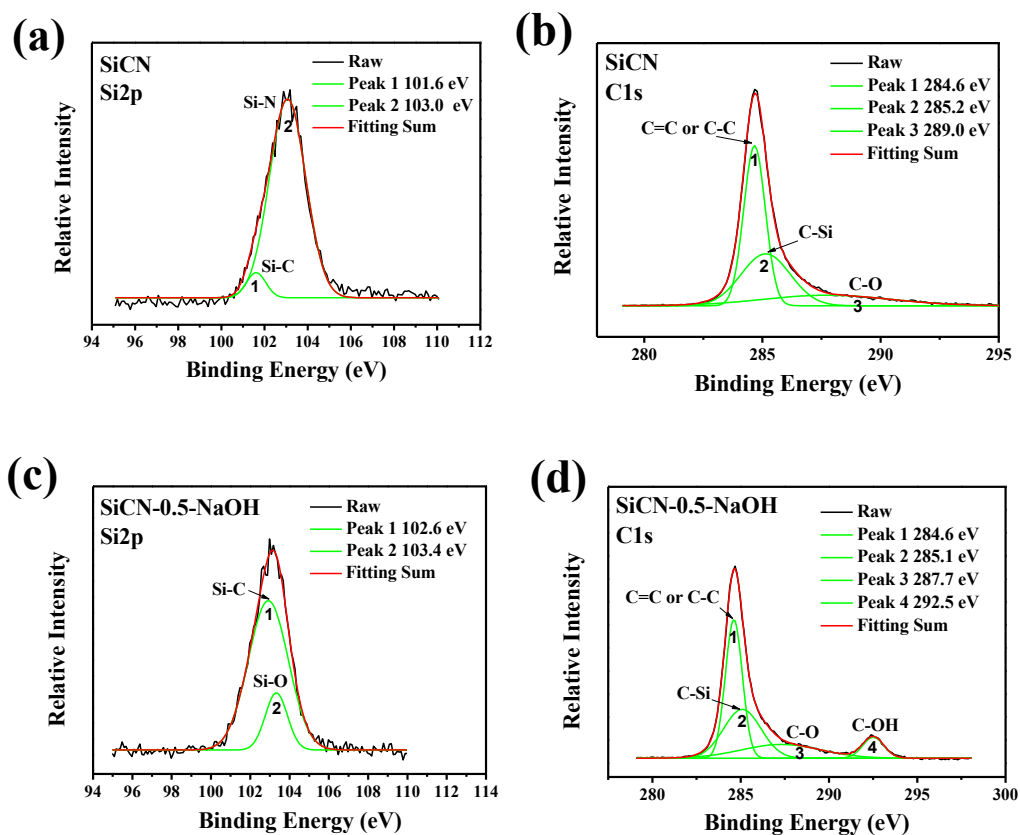


**Figure 4.** XPS analysis of SiCN in the Si2p (a) and C1s (b) regions; XPS analysis of NaOH-treated SiCN-0.5-NaOH in the Si2p (c) and C1s (d) regions.

**Table 1.** Atomic percent of elements on the surface of SiCN and SiCN-0.5-NaOH materials determined by XPS analysis.

Samples	In atomic percent from XPS				
	Si	C	N	O	Na
SiCN	14.33	71.27	13.19	1.21	0
SiCN-0.5-NaOH	6.03	72.90	2.13	16.43	2.51

XPS analysis is employed to compare the element valences in SiCN before and after NaOH-treating. There is no evident Si-N peak observed for the treated SiCN material (SiCN-0.5-NaOH, Figure 4c). However, an intense Si-C peak increase and a new Si-O peak

arises in the XPS spectrum of pristine SiCN (Figure 4a). It is clear evidence that NaOH reacts with  $\text{Si}_3\text{N}_4$  to form a compound containing silicon, carbon and trace of oxygen and sodium. This can be further investigated by the atomic percent analysis of elements on the surface of SiCN materials, the result of which is shown in Table 1. By comparing the element contents before and after NaOH treatment, we can conclude that both oxygen and sodium contents were increased, while the silicon and nitrogen contents were decreased after the NaOH treatment, a possible explanation is the former is gained from NaOH and the latter is lost because of the  $\text{Si}_3\text{N}_4$  removal. In addition, the change of carbon content before and after NaOH-treating is not dramatically, which hints the carbon is unlikely be involved in the evaporated may not take part for the chemical reaction of NaOH with SiCN. It is also interesting to compare the fitting C1s spectra (Figure 4b and 4d). C=C or C-C, Si-C and C-O peaks are all exhibited in both treated and untreated spectra, however, the C-OH peak exists only after NaOH treating which implied the -OH from the NaOH solution during treating process is responsible for the -OH group in the final product.

From above TEM, FTIR and XPS analysis, it strongly suggests that the  $\text{Si}_3\text{N}_4$  phase is removed by NaOH. The reaction of  $\text{Si}_3\text{N}_4$  and NaOH in molecular level is schematically shown in Figure 5.

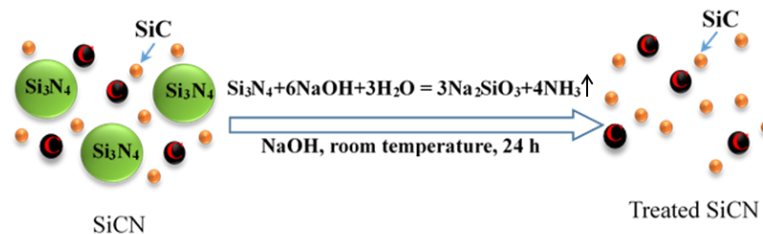


**Figure 5.** Schematic representation of the molecular level interface of the reaction of SiCN and NaOH.

As a side effect of above reaction, there are a lot of voids lefts in the SiCN structure,

which is consistent with the SEM and TEM observation (Figure 2 and 3). The surface pattern change has profound influence on the electrochemical behavior of the materials. The micro-cracks which emerged into the surface of the NaOH-treated SiCN materials is instrumental in offering  $\text{Li}^+$  conduct channels, and buffer the volume expansion simultaneously during the charge-discharge process. However, large cracks may bring structure damage during  $\text{Li}^+$  intercalation/deintercalation. Therefore, appropriate size of cracks is a balance between the transportation and structure strength and is important for the electrochemical performance of anode material, which will be discuss in the following part of electrochemical measurements (Figure 6-10).

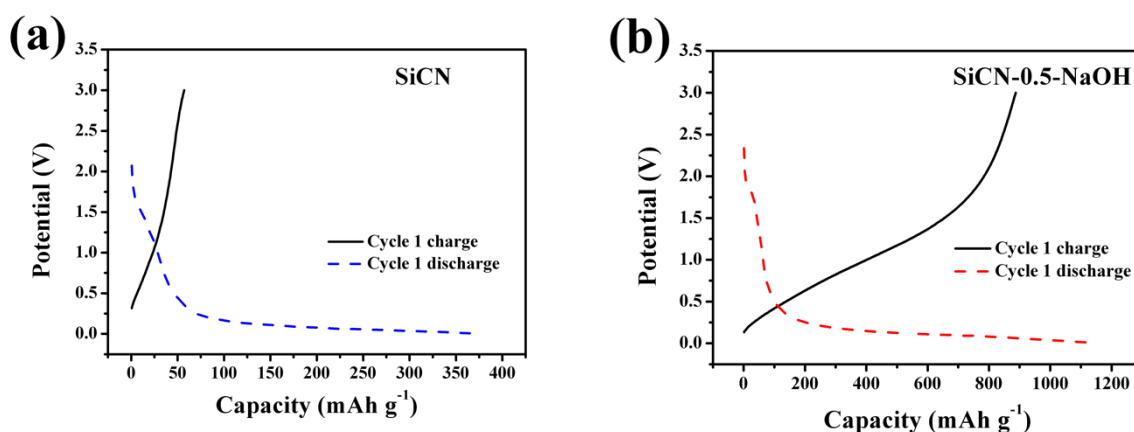


**Figure 6.** The capacity-potential curves of the first cycle for SiCN (a) and SiCN-0.5-NaOH (b) anodes at a current density of  $40 \text{ mA g}^{-1}$ .

Figure 6 presents the cycling performance of SiCN and SiCN-0.5-NaOH anodes at the first cycle where the charge and discharge potential curves are plotted against capacity. As Figure 6 shows, the charge-discharge potential curves of both the SiCN and SiCN-0.5-NaOH anodes display gentle slopes demonstrating their amorphous structures, which are consistent with the XRD patterns in Figure 1c. The charge and discharge potential plateaus of untreated SiCN is short (Figure 6a), which indicates low capacity, while the charge and discharge potential plateaus of SiCN-0.5-NaOH anode (Figure 6b) are significantly longer than that of untreated SiCN, which manifests higher capacity. The discharge potential plateau for the SiCN-0.5-NaOH anode in the first cycle is about 1.7 V while no such plateau exhibits in the same range in the curve of SiCN anode, indicating there may be a unique phase transformation on the surface of NaOH-treated SiCN during discharge process.

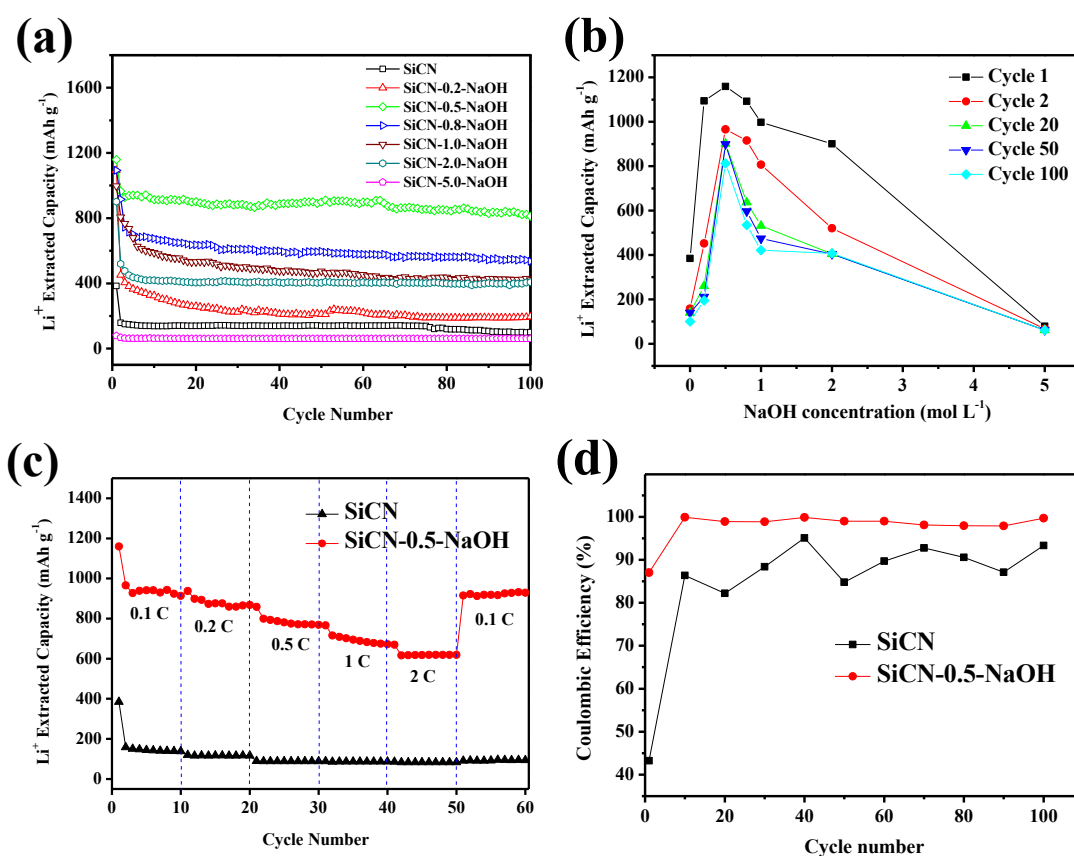


**Figure 7.** (a) Cycle performances of the SiCN and SiCN-x-NaOH (x=0.2, 0.5, 0.8, 1.0, 2.0, 5.0) anodes at a charge-discharge current density of 40 mA g<sup>-1</sup>; (b) graphs of the extracted capacity vs. NaOH concentration for SiCN-x-NaOH (x=0.2, 0.5, 0.8, 1.0, 2.0, 5.0) anodes at cycle 1, 2, 20, 50 and 100; (c) high-rate performances of SiCN and SiCN-0.5-NaOH anodes at charge-discharge current densities of 0.1, 0.2, 0.5, 1 and 2 C (1 C=400 mA g<sup>-1</sup>); (d) graphs of the coulombic efficiency vs. cycle number for the SiCN and SiCN-0.5-NaOH anodes.

Figure 7a shows the cycle performances of the SiCN and SiCN-x-NaOH (x=0.2, 0.5, 0.8, 1.0, 2.0, 5.0) anodes at a charge-discharge current density of 40 mA g<sup>-1</sup>. The initial specific de-insertion capacities of the NaOH-treated SiCN are 1093.9, 1159.5, 1092.8, 997.7, 900.9, 78.7 mAh g<sup>-1</sup>, respectively. The NaOH-treated SiCN anode are giving much higher capacity than the pristine SiCN anode (384.1 mAh g<sup>-1</sup>), except for the SiCN-5.0-NaOH treated anode. It is remarkable that the treated SiCN exhibit fundamentally improved cycling stability. The cycling stability of untreated SiCN anode is less satisfying, where capacity drops

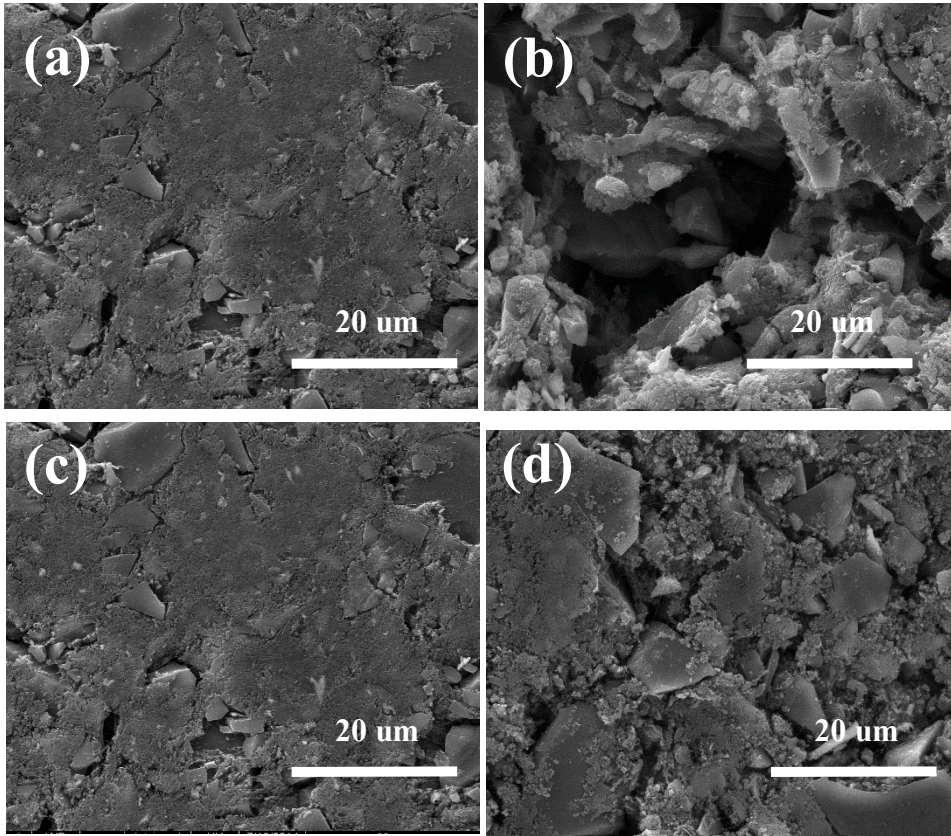
dramatically to  $50 \text{ mAh g}^{-1}$  from the 2<sup>nd</sup> cycle, However, the capacity decay for most of the treated SiCN materials is acceptable. Some treated samples show outstanding performance, among which, the SiCN-0.5-NaOH anode shows the best cycle stability and reversible capacity. While the first de-inserted capacity of the SiCN-0.5-NaOH anode ( $1159.5 \text{ mAh g}^{-1}$ ) is 3 times better than the untreated SiCN anode ( $384.1 \text{ mAh g}^{-1}$ ), the cycling stability is fundamentally improved with a decay as little as 16.7% at the second cycle. The capacity at the second cycle is still up to  $965.3 \text{ mAh g}^{-1}$  and the cycling performance is considered to be stable above  $900 \text{ mAh g}^{-1}$  from the 3<sup>rd</sup> to 50<sup>th</sup> cycle. Even after 100 cycles, the extracted capacity of the SiCN-0.5-NaOH anode is still up to  $812.3 \text{ mAh g}^{-1}$ , which is 8.1 times greater than the untreated SiCN anode ( $100.4 \text{ mAh g}^{-1}$ ), and 3.1 times as large as the traditional graphite anode. The excellent electrochemical performance attributes to the ceramic structure of NaOH treated SiCN, hence the electrode materials are tolerant to pulverization after many cycles. The explanations are supported by SEM. The SEM images of the SiCN and SiCN-0.5-NaOH anodes before and after cycling are shown in Figure 8, the material pulverization can be clearly seen in the untreated SiCN anode after several cycles. Meanwhile, the pulverization of the SiCN-0.5-NaOH anode is negligible.

Figure 7b shows the dependence of extracted capacity *vs.* NaOH concentration for the SiCN anodes in different charging/discharging cycles. From the graphs, we can see that the SiCN materials treated with  $0.2\text{-}1.0 \text{ mol L}^{-1}$  NaOH have better capacity than SiCN without NaOH treating. The SiCN-0.5-NaOH anode exhibits the best cycle stability, indicating it may have an appropriate number and size of cracks for  $\text{Li}^+$  transport. However, the SiCN-5.0-NaOH anode has the worst capacity and cycle stability, which is even worse than

the untreated SiCN anode. A possible explanation is that the treating with high concentration of NaOH ( $5 \text{ mol L}^{-1}$ ) damages the network of SiCN material and results in poor electrochemical performance structure. Hence, the NaOH concentration for SiCN treating is a key factor for obtaining good electrochemical performance. For this work, the optimal NaOH concentration concluded is in the proximity of  $0.5 \text{ mol L}^{-1}$ .

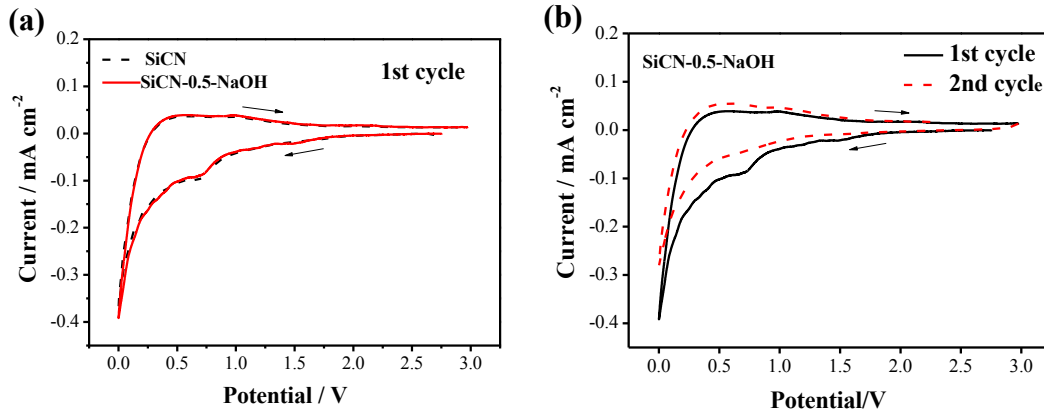
Figure 7c shows the high-rate performances of the SiCN and SiCN-0.5-NaOH anodes at different current densities of 0.1, 0.2, 0.5, 1 and 2 C (1 C= $400 \text{ mA g}^{-1}$ ). As shown, the SiCN-0.5-NaOH anode has excellent electrochemical performance at high rates especially comparing with the untreated SiCN anode. The SiCN-0.5-NaOH anode delivered a capacity of 1159.5, 937.9, 857.8, 766.1 and  $668.9 \text{ mAh g}^{-1}$  at 0.1, 0.2, 0.5, 1 and 2 C, respectively, suggesting complete recovery of the first cycle capacity of around  $915.2 \text{ mAh g}^{-1}$  when the current rate was brought back to 0.1 C. In contrast, the untreated SiCN anode shows less satisfying capacity that is below  $100 \text{ mAh g}^{-1}$  under the same charge-discharge rates. From these results, it is demonstrated that NaOH-treating improves the high-rate capability of SiCN anode dramatically.

Figure 8d shows the coulombic efficiency (%) of SiCN and SiCN-0.5-NaOH at 1-100 charge-discharge cycles. Except for the first cycle, the coulombic efficiency of SiCN-0.5-NaOH is about 97-100%, and the average coulombic efficiency is 97.83 % which is higher than that of SiCN (93.43%), indicating NaOH treating improves the coulombic efficiency of SiCN anode.



**Figure 8.** SEM images of the untreated SiCN anode before (a) and after (b) charge-discharge cycling; the SiCN-0.5-NaOH anode before (c) and after (d) charge-discharge cycling.

CV profiles of untreated SiCN and SiCN-0.5-NaOH anodes in the first scanning cycle are shown in Figure 9a. An evident cathodic peak is located at around 0.7 V and can be attributed to the formation of a solid electrolyte interphase (SEI). The SEI usually occurs on the electrode surface at the first few cycles due to the reaction of electrode material and electrolyte, and typically results in irreversible capacity [6]. From Figure 9b, the peak indicating the SEI formation occurred in the first scanning cycle. The peak areas decrease with increasing the cycle number, indicating the loss of extracted capacity.



**Figure 9.** (a) Cyclic voltammetry curves of SiCN and SiCN-0.5-NaOH anodes at a scan rate of  $0.05 \text{ mV s}^{-1}$  for the first cycle; (b) Cyclic voltammetry curves of SiCN-0.5-NaOH anodes at a scan rate of  $0.05 \text{ mV s}^{-1}$  for the first and second cycles.

As Figure 10 shows, EIS tests were carried out to evaluate the electrochemical kinetics properties of the untreated SiCN and SiCN-0.5-NaOH materials at 50% depth of discharge (DOD). The Nyquist plots for both electrodes consist of two semicircles and a straight line, corresponding to a high-frequency semicircle, an intermediate-frequency semicircle and a low-frequency straight line associated with the diffusion process of lithium ions in anode (a Warburg region). The smaller semicircle for SiCN-0.5-NaOH anode indicates a lower electrochemical resistance than untreated SiCN anode [34]. The results were fitted to an electrochemical model using ZView module from Sai software [24, 25] set. The fitting model is an equivalent circuit electrochemical model, which is depicted, in the inserted figure of Figure 10.  $R_s$  at the high-frequency intercept on the real axis represented bulk resistance depending on electrolyte solution, active material, and current collector and so on.  $R1$  at high frequency was the migration resistance of lithium ion through the SEI, while  $R2$  at middle frequency was the charge transfer resistance in the anode-electrolyte interface, both arcs are associated with the interface between the electrolyte and the active particles [35, 36]. The constant phase element ( $CPE1$  and  $CPE2$ ) replaces the conventional

double-layer and passivation film capacitance [37]. Table 2 shows the EIS fitting results of SiCN and SiCN-0.5-NaOH anodes. Compared to untreated SiCN, SiCN-0.5-NaOH anode demonstrated smaller  $R1$  value, which indicates faster electrochemical kinetics, corresponded with high-rate performance.

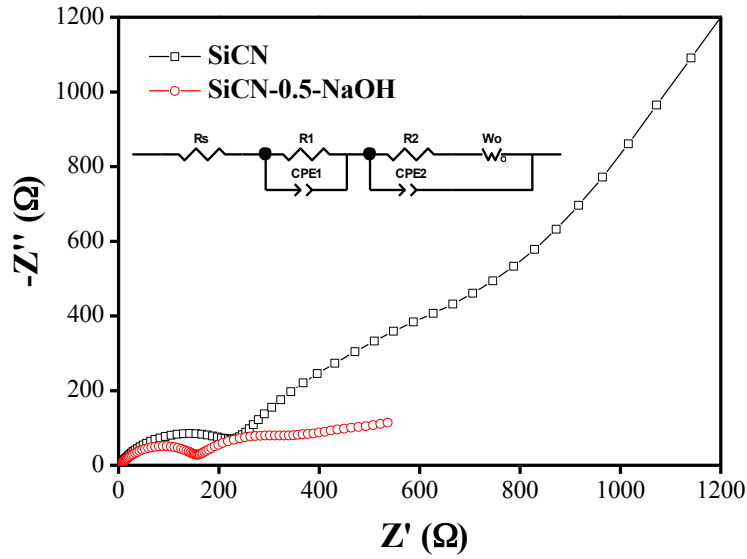


**Figure 10.** EIS Nyquist plots of experimental data of SiCN and SiCN-0.5-NaOH anodes (The inserted figure is the equivalent circuit for EIS data fitting).

**Table 2.** EIS fitting results of SiCN and SiCN-0.5-NaOH anode.

Parameter	SiCN	SiCN-0.5-NaOH
$R_s / \Omega$	5.368	5.522
$R1 / \Omega$	233.6	152.6
$R2 / \Omega$	675.3	$1.01 \times 10^{-5}$
$CPE1-T / \mu F$	14.83	20.93
$CPE2-T / \mu F$	251.61	820.46
$W_0-R / \Omega$	233.7	477.6

There are three reasons for good electrochemical performance of NaOH-treated SiCN anodes: 1) the nonconductive  $Si_3N_4$  phase has been removed by NaOH treating as evidenced by TEM, XPS and FTIR results; 2) the micro-sized cracks not only provide new channels for the insertion or extraction of  $Li^+$  but also buffer the detrimental effects of the

large volume changes, resulting in improved capacity and enhanced cycling stability; 3) the rich carbon which embeds in the SiCN matrix can not only offer more active sites for lithium ion storage, but also may make the material structure more stable than carbon-less material, forming a continuous network for the storage of lithium ions.

In this work, we conclude that detailed control over the characters of anode, the number of pores and cracks in SiCN matrix are important to improve the electrochemical performance. The pores and cracks can be easily adjusted by the pore-forming solution concentration and reaction time. Because the dependence of performance on crack number/size is monotonic, the detailed control over number of pores and cracks is helpful to adopt the most appropriate preparation conditions. The appropriate number and sizes of cracks can not only improve efficient  $\text{Li}^+$  transfer but also promise a better structural stability of SiCN matrix during cycling.

The process of our NaOH-treating for SiCN materials involves no highly toxic chemical reagent and it is easy to operate for practical use. Compared with HF-treating for porous SiCN which we have done before [25], our NaOH-treating is safer and more environmental-friendly, and even the electrochemical performance of NaOH-treating SiCN is better than HF-treating one. Therefore, our treating method for micro-cracked or porous SiCN materials can be generalized to other Si-based material anodes for the application of Li-ion batteries.

### **3. Experimental Section**

#### *3.1 Reagents and chemicals*

Diphenyldichlorosilane and dichloromethylvinylsilane were purchased from Alfa-Asear

Corp., US and used without purification. Ethylenediamine (EDA), triethylamine (TEA), toluene, hydrofluoric acid, 2, 2-azo-bis-iso-butyronitrile (AIBN) and sodium hydroxide (NaOH) solid were purchased from Tianjin Kewei Corp., China. The water present in EDA, TDA, and toluene was removed by distillation prior to use. AIBN were used without purification.

### *3.2 Preparation of the polymer-derived SiCN*

The polymer-derived SiCN material was prepared by pyrolyzing a poly(diphenylsilylcarbodiimide) precursor, which was synthesized by the aminolysis reaction of EDA, TDA and dichlorosilanes. The synthesis details are as following: a solution of EDA (4.81 g, 0.08 mol) and TEA (16.16 g, 0.16 mol) in 100 mL toluene was placed in a 500 mL three-neck round bottom flask fitted with a reflux condenser, a dropping funnel and an argon inlet. The mixed solution was magnetically stirred. To this solution, dichloromethylsilane (8.38 mL, 0.04 mol) and dichloromethylvinylsilane (5.18 mL, 0.04 mol) in 50 mL toluene was then added slowly from the dropping funnel (about 40 min) to keep the reaction temperature below 40 °C. The reaction mixture was refluxed at 60 °C for 40 min, and then refluxed at 100 °C for 90 min. After that, the reaction mixture was cooled to ambient temperature. All the reaction was under argon atmosphere. The triethylamine hydrochloride  $N(C_2H_5)_3 \cdot HCl$  salt was filtered off and the filtrate was rotaevaporated to remove the solvent and other volatile components. The remaining yellow oil was dried at room temperature under argon atmosphere overnight to obtain poly(diphenylsilylcarbodiimide) precursor. Then the as-prepared poly(silylcarbodiimide) precursor was cross-linked into a colloidal solid at 80 °C using AIBN as a radical initiator.

Then the cross-linked precursor were placed in an  $\text{Al}_2\text{O}_3$  crucible and pyrolyzed in an alumina tube furnace in an argon flow at  $1000\text{ }^\circ\text{C}$  for 1 h at a heating rate of  $5\text{ }^\circ\text{C}/\text{min}$ . Then the as-prepared SiCN were powdered and sieved with a 200-meshed standard sieve.

### 3.3 Removing $\text{Si}_3\text{N}_4$ from SiCN matrix

Treating of the SiCN powders was conducted by using different concentration of NaOH aqueous solution. 1.0 g of the as-prepared SiCN powders was put into  $0.2\text{--}5.0\text{ mol L}^{-1}$  20 ml NaOH aqueous solution in a Teflon container. The mixture was stirred at room temperature for 24 h, then filtered and washed with distilled water to remove any excess. The sample was dried in an oven at  $100\text{ }^\circ\text{C}$  for 24 h. For convenience, we use the denotation of SiCN-x-NaOH ( $x=0.2, 0.5, 0.8, 1.0, 2.0, 5.0$ ) for the samples treated by 0.2, 0.5, 0.8, 1.0, 2.0 and  $5.0\text{ mol L}^{-1}$  NaOH solution, respectively. The chemical synthesis route is shown in Figure 11.

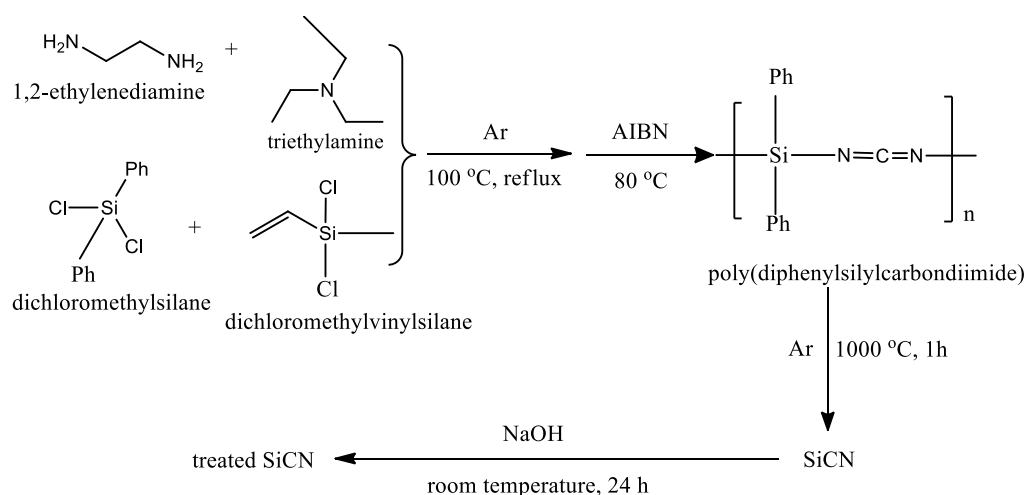


**Figure 11.** Schematic procedure for the synthesis of NaOH-treated SiCN materials.

### 3.4 Material characterization

The structural morphologies of these NaOH-treated SiCN materials were characterized with a scanning electron microscopy system (SEM, FEI Nova Nano 230) with an

accelerating voltage of 15 kV and a transmission electron microscope system (TEM, FEI Tecnai G<sup>2</sup> F20, Philips, Eindhoven, the Netherlands) operating at 200 kV. Thermogravimetric analyses (TGA) and Differential Scanning Calorimetry (DSC) were conducted under argon atmosphere with a TGA Q500 system (TA, US). Fourier transform infrared (FTIR) spectra were collected by a Nicolet IR200 automatic infrared spectrometer (Thermo, US) using the KBr pellet method. The X-ray powder diffraction patterns were recorded on a Rigaku D8A X-ray diffractometer (Bruker, Germany) and Cu K $\alpha$  radiation ( $\lambda = 0.1540$  nm) in the  $2\theta$  range of 10-80°. The XPS measurements were carried out with an X-ray photoelectron spectrometer (Thermo fisher) using a monochromatic Al K $\alpha$  (1486.7 eV) source at a voltage of 15 kV and an emission current of 10 mA. Brunner-Emmet-Teller (BET) measurements was analyzed by an ASAP2020 analyzer (Micromeritics, USA) at liquid nitrogen temperature.

### *3.5 Electrochemical measurements*

The as-prepared SiCN powders were used as the anode materials for lithium ion batteries. The anode electrodes were fabricated by mixing the powdered active material (untreated SiCN, SiCN-0.2-NaOH, SiCN-0.5-NaOH, SiCN-0.8-NaOH, SiCN-1.0-NaOH and SiCN-5.0-NaOH, respectively) with acetylene black (ENSACO, Switzerland) and polytetrafluoroethylene (PTFE, Sigma-Aldrich, Switzerland) binder in the weight ratios of 70:20:10. The testing coin-type cells (size: CR 2032) were assembled in an argon filled glove box, with the as-prepared anodes, Li foil as counter and reference electrodes, Celgard 2300 (Celgard, Charlotte, NC) film separator and 1.15 M LiPF<sub>6</sub> in 1:1:1 (by volume) ethylene carbonate (EC)/propylene carbonate (PC)/dimethyl carbonate (DMC) electrolyte.

The active material content in the electrode was approximately 5.0 mg. Galvanostatic charge-discharge cycle tests were carried out on a LAND 2001A battery testing system (Wuhan Jinnuo Corp., China) at current densities of 0.1C, 0.2C, 0.5C, 1C and 2C (1C=400 mAh g<sup>-1</sup>) in the potential range of 0.0-3.0 V vs. Li<sup>+</sup>/Li.

The cyclic voltammetry (CV) test was performed on an electrochemical workstation (Solartron 1287, Solartron Metrology Corp., UK) at scan rate of 0.05 mV s<sup>-1</sup> with the potential range from 0.0 to 3.0 V.

The electrochemical impedance (EIS) was conducted by an electrochemical workstation (CHI 604E, Chenhua Corp., Shanghai, China) with the frequency range from 10 mHz to 100 KHz. All the tests were performed at room temperature.

#### **4. Conclusion**

The high-conductive SiCN materials have been synthesized by pyrolysis and NaOH post treatment of carbon-rich poly(diphenylsilycarbodiimide). The whole prepare process are easy to handle and involves no highly toxic chemical reagents. The nonconductive Si<sub>3</sub>N<sub>4</sub> phase of SiCN matrix is successful remove by NaOH-treating process. The treated materials show excellent electrochemical properties as anodes for lithium ion batteries. Especially, treating SiCN with 0.5 mol L<sup>-1</sup> of NaOH aqueous solution results in the best performances. The initial extracted capacity, the Coulombic efficiency, reversible capacity and the high-rate capability have been prominently improved by the NaOH treating. The outstanding electrochemical performance of SiCN-0.5-NaOH anode is ascribed to removing of nonconductive Si<sub>3</sub>N<sub>4</sub> phase and the formation of micro-sized cracks on the material rough surface which can offer enough channels for Li<sup>+</sup> transfer and alleviate the structural collapse

during charge-discharge cycling. The chemical synthesis and post-treating method reported in this work represents a new improved method for the preparation of general polymer-derived silicon-based material electrodes with high electrochemical performance for lithium ion batteries.

### **Acknowledgements**

The authors acknowledge the financial supports from the National Natural Science Foundation of China (no. 21103124), Tianjin Municipal Education Commission Fund for Outstanding Young College Teachers (no. ZX10QN047) and the Program for Innovative Research Team in Universities of Tianjin (no. TD12-5038).

### **Conflicts of Interest**

The authors declare no conflict of interest.

### **References**

- 1 Goodenough, J. B.; Park, K. S. The Li-ion Rechargeable Battery: A Perspective. *J. Am. Chem. Soc.* **2013**, *135*, 1167-1176.
- 2 Choi, N. S.; Chen, Z.; Freunberger, S. A.; Ji, X.; Sun, Y. K.; Amine, K.; Yushin, G.; Nazar, L. F.; Cho, J. P.; Bruce, G. Challenges Facing Lithium Batteries and Electrical Double-Layer Capacitors. *Angew. Chem. Int. Ed.* **2012**, *51*, 9994-10024.
- 3 Armand, M.; Tarascon, J.-M. Building better batteries. *Nature* **2008**, *451*, 652-657.
- 4 Bai, Y.; Tang, Y.; Wang, Z. H.; Zhe, J.; Wu, F.; Wu, C.; Liu, G. Electrochemical performance of Si/CeO<sub>2</sub>/Polyaniline composites as anode materials for lithium ion batteries. *Solid State Ionics* **2015**, *272*, 24-29.
- 5 Feng, C. H.; Zhang, L.; Yang, M. H.; Song, X. Y.; Zhao, H.; Jia, Z.; Sun, K. N.; Liu, G. One-pot Synthesis of Copper Sulfide Nanowires/reduced Graphene Oxide Nanocomposites with Excellent Lithium-storage Properties as Anode Materials for Lithium-ion batteries. *ACS App. Mater. Interfaces* **2015**, *7*, 15726-15734.
- 6 Dahn, J. R.; Zheng, T.; Liu, Y. Xue, Mechanisms for Lithium Insertion in Carbonaceous Materials. *J. S. Science* **1995**, *270*, 590-593.
- 7 Dahn, J. R.; Wilson, A. M.; Xing, W. B.; Zank, G. A. Electrodes for Lithium Ion Batteries using Polysilazanes Ceramic with Lithium. *US Patent* **1997**, 56311064.

- 8 Dahn, J. R.; Wilson, A. M.; Xing, W. B.; Zank, G. A. Electrodes for Lithium Ion Batteries using Polysilazanes. *European Patent* **1997**, 0813259A1.
- 9 Kolb, R.; Fasel, C.; Kunzmann, V. L.; Riedel, R. SiCN/C-ceramic Composite as Anode Material for Lithium Ion Batteries. *J. Eur. Ceram. Soc.* **2006**, *26*, 3903-3908.
- 10 Su, D.; Li, Y. L.; Feng, Y.; Jin, J. Electrochemical Properties of Polymer-Derived SiCN Materials as the Anode in Lithium Ion Batteries. *J. Am. Ceram. Soc.* **2009**, *92*, 2962-2968.
- 11 Graczyk-Zajac, M.; Mera, G.; Kaspar, J.; Riedel, R. Electrochemical Studies of Carbon-rich Polymer-derived SiCN Ceramics as Anode Materials for Lithium-ion Batteries *J. Eur. Ceram. Soc.* **2010**, *30* 3235-3243.
- 12 Kaspar, J.; Mera, G.; Nowak, A. P.; Graczyk-Zajac, M.; Riedel, R. Electrochemical Study of Lithium Insertion into Carbon-rich Polymer-derived Silicon Carbonitride Ceramics. *Electrochim. Acta* **2010**, *56*, 174-182.
- 13 Gracyk-Zajac, M.; Fasel, C.; Riedel, R. Polymer-derived-SiCN ceramic/graphite Composite as Anode Material with Enhanced Rate Capability for Lithium Ion Batteries. *J. Power Sources* **2011**, *196*, 6412-6418.
- 14 Chen, Y.; Li, C.; Wang, Y.; Zhang, Q.; Xu, C.; Wei, B.; An, L. Self-assembled Carbon-silicon Carbonitride Nanocomposites: High performance Anode Materials for Lithium-ion Batteries. *J. Mater. Chem.* **2011**, *21*, 18186-18190.
- 15 Bhandavat, R.; Singh, G. Improved Electrochemical Capacity of Precursor-Derived Si(B)CN Carbon Nanotube Composite as Li-ion Battery Anode. *ACS Appl. Mater. Inter.* **2012**, *4*, 5092-5097.
- 16 Liu, G.; Kaspar, J.; Reinold, L. M.; Gracyk-Zajac, M.; Riedel, R. Electrochemical Performance of DVB-modified SiOC and SiCN Polymer-derived Negative Electrodes for Lithium-ion Batteries. *Electrochim. Acta* **2013**, *106*, 101-108.
- 17 Reinold, L. M.; Graczyk-Zajac, M.; Gao, Y.; Mera, G.; Riedel, R. Carbon-rich SiCN Ceramics as High Capacity/High Stability Anode Material for Lithium-ion Batteries. *J. Power Sources* **2013**, *236*, 224-229.
- 18 Wilamowska, M.; Graczyk-Zajac, M.; Riedel, R. Composite Materials Based on Polymer-derived SiCN Ceramic and Disordered Hard Carbons as Anodes for Lithium-ion Batteries. *J. Power Sources* **2013**, *244*, 80-86.
- 19 Baek, S. H.; Reinold, L. M.; Graczyk-Zajac, M.; Riedel, R.; Hammerath, F.; Büchner, B.; Grafe, H. J. Lithium Dynamics in Carbon-rich Polymer-derived SiCN Ceramics Probed by Nuclear Magnetic Resonance. *J. Power Sources* **2014**, *253*, 342-348.
- 20 Nowak, A. P.; Wicikowska, B.; Lisowska-Oleksiak, A. New Ceramic Materials Derived from Pyrolyzed Poly(1,2-dimethylsilazane) and Starch as a Potential Anode for Li-ion Batteries. *Solid State Ionics* **2014**, *263*, 131-139.
- 21 Feng, Y. Electrochemical Properties of Heat-treated Polymer-derived SiCN Anode for

- Lithium Ion Batteries. *Electrochim. Acta* **2010**, *55*, 5860-5866.
- 22 Feng, Y.; Du, G. X.; Zhao, X. J.; Yang, E. C. Preparation and Electrochemical Performance of SiCN-CNTs Composite Anode Material for Lithium Ion Batteries *J. Appl. Electrochem.* **2011**, *41*, 999-1002.
  - 23 Feng, Y.; Feng, N. N.; Du, G. X. Preparation and Electrochemical Performance of Polymer-derived SiCN-graphite Composite as Anode Material for Lithium Ion Batteries. *Int. J. Electrochem. Sci.* **2012**, *7*, 3135-3140.
  - 24 Feng, Y.; Feng, N. N.; Wei, Y. Z.; Bai, Y. Preparation and Improved Electrochemical Performance of SiCN-graphene Composite Derived From Poly(silylcarbodiimide) as Li-ion Battery Anode. *J. Mater. Chem. A* **2014**, *2*, 4168-4177.
  - 25 Feng, N. N.; Feng, Y.; Wei, Y. Z.; Zhou, X. P. Preparation and Electrochemical Performance of A Porous Polymer-derived Silicon Carbonitride Anode by Hydrofluoric Acid Etching for Lithium Ion Batteries. *RSC Adv.* **2014**, *4*, 23694-23702.
  - 26 Ionescu, E.; Kleebe, H. J.; Riedel, R. Silicon-containing Polymer-derived Ceramic Nanocomposites (PDC-NCs): Preparative Approaches and Properties. *Chem. Soc. Rev.* **2012**, *41*, 5032-5052.
  - 27 Colombo, P.; Mera, G.; Riedel, R.; Sorarù, G. D. Polymer-Derived Ceramics: 40 Years of Research and Innovation in Advanced Ceramics. *J. Am. Ceram. Soc.* **2010**, *93*, 1805-1837.
  - 28 Gottardo, L.; Bernard, S.; Gervais, C.; Weinmann, M.; Miele, P. Study of the Intermediate Pyrolysis Steps and Mechanism Identification of Polymer-derived SiBCN Ceramics. *J. Mater. Chem.* **2012**, *22*, 17923-17933.
  - 29 Sarkar, S.; Gan, Z.; An, L.; Zhai, L. Structural Evolution of Polymer-Derived Amorphous SiBCN Ceramics at High Temperature. *J. Phys. Chem. C* **2011**, *115*, 24993-25000.
  - 30 Widgeon, Mera, S. Gao, G. Y.; Sen, S.; Navrotsky, A.; Riedel, R. Effect of Precursor on Speciation and Nanostructure of SiBCN Polymer Derived Ceramics. *J. Am. Ceram. Soc.* **2013**, *96*, 1651-1659.
  - 31 Mera, G.; Navrotsky, A.; Sen, S.; Kleebe, H. J.; Riedel, R. Polymr-derived SiCN and SiOC Ceramics-structure and Energetics at the Nanoscale. *J. Mater. Chem. A* **2013**, *1*, 3826-3836.
  - 32 Mera, G.; Riedel, R.; Poli, F.; Müller, K. Carbon-rich SiCN Ceramics Derived from Phenyl-containing Poly(silylcarbodiimides). *J. Eur. Ceram. Soc.* **2009**, *29*, 2873-2883.
  - 33 Widgeon, S.; Mera, G.; Gao, Y.; Stoyanov, E.; Sen, Navrotsky, S. A.; Riedel, R. Nanostructure and Energetics of Carbon-Rich SiCN Ceramics Derived from Polysilylcarbodiimides: Role of the Nanodomain Interfaces. *Chem. Mater.* **2012**, *24*, 1181-1191.
  - 34 Woo, J. J.; Maroni, V. A.; Liu, G.; Vaughey, J. T.; Gosztola, D. J.; Amine, K.; Zhang,

- Z. C. Symmetrical Impedance Study on Inactivation Induced Degradation of Lithium Electrodes for Batteries Beyond Lithium-Ion. *J. Electrochem. Soc.* **2014**, *161*, A827-830.
- 35 Swietoslowski, M.; Molenda, M.; Grabowska, M.; Wach, A.; Kustrowski, P.; Dziembai, R. Electrochemical Impedance Spectroscopy Study of C/Li<sub>2</sub>MnSiO<sub>4</sub> Composite Cathode Material at Different States of Charge. *Solid State Ionics* **2014**, *263*, 99-102.
- 36 Hang, T.; Mukoyama, D.; Nara, H.; Takami, N.; Momma, T.; Osaka, T. Electrochemical Impedance Spectroscopy Analysis for Lithium-ion Battery Using Li<sub>4</sub>Ti<sub>5</sub>O<sub>12</sub> Anode. *J. Power Sources* **2013**, *222*, 442-447.
- 37 Srinivasan, A.; Shin, K. S.; Rajendran, N. Dynamic Electrochemical Impedance Spectroscopy (DEIS) Studies of AZ31 Magnesium Alloy in Simulated Body Fluid Solution. *RSC Adv.* **2014**, *4*, 27791-27795.